European Congress on Computational Methods in Applied Sciences and Engineering
ECCOMAS 2000
Barcelona, 11-14 September 2000

Multiobjective Aerodynamic Optimization of Supersonic Wings Using Navier-Stokes Equations

Daisuke Sasaki[*], Shigeru Obayashi[*], Keisuke Sawada[*] and Ryutaro Himeno[†]

[*]Tohoku University, Department of Aeronautics and Space Engineering,
Sendai, 980-8579, Japan
e-mail: sasaki@ad.mech.tohoku.ac.jp, obayashi@ieee.org
web page: http://www.ad.mech.tohoku.ac.jp/index.html

[†]The Institute of Physical and Chemical Research (RIKEN),
Wako, 351-0198, Japan
e-mail: himeno@postman.riken.go.jp, web page: http://w3cic.riken.go.jp

Key Words: Genetic Algorithms, Multiobjective Optimization, Aerodynamic Design, Supersonic Wing, Navier-Stokes Equations

Abstract. *The design optimization of a wing for supersonic transport by means of Multiobjective Genetic Algorithm (MOGA) is presented. The objective function is to minimize the drag for transonic cruise, the drag for supersonic cruise and the bending moment at the wing root for the supersonic condition. The wing shape is defined by planform, thickness distributions and warp shapes, in total of 66 design variables. A Navier-Stokes code is used to evaluate the aerodynamic performance at both cruise conditions. CFD computations are parallelized by a simple master-slave concept on FUJITSU VPP-700E supercomputer system at The Institute of Physical and Chemical Research. Consequently, the Pareto solutions are obtained in the three-dimensional objective function space. The resultant Pareto solutions are compared with the wing designed by National Aerospace Laboratory as well as the optimal wing obtained previously under the inviscid flow.*

1 INTRODUCTION

Demand for developing a new Supersonic Transport (SST) is expected to become larger, because people travel overseas more frequently. Last ten years, several efforts have been made to develop a new SST in the States, Europe and Japan. In Japan, National Aerospace Laboratory (NAL) is studying and designing a SST to launch the small supersonic experimental airplane[1] in 2002.

Considering a new SST design, there exist many technical difficulties to overcome. L/D must be improved, and the sonic boom should be prevented. However, there is a severe tradeoff between lowering the drag and boom. As a result, a new SST is expected to cruise at a supersonic speed only over the sea and to cruise at a transonic speed over the land. This means that the important design objectives are not only to improve a supersonic cruise performance but also to improve a transonic one. For example, a large sweep angle can reduce the wave drag, but it limits the allowable aspect ratio due to structural problems. Therefore, there are many tradeoffs to be addressed in designing a SST.

To identify global tradeoffs, the problem can be treated as multiobjective (MO) optimization. MO optimization seeks to optimize the components of a vector-valued objective function. In general, the solution to this problem is not a single point unlike single objective optimization, but a family of points known as the Pareto-optimal set. Pareto solutions, which are members of the Pareto-optimal set, represent tradeoffs among multiple objectives. Multiobjective Genetic Algorithms (MOGAs) are unique optimization methods to sample multiple Pareto solutions efficiently and effectively.[2] GAs are the optimization methods that imitate the natural evolution. Since GAs seek optimal solutions in parallel using a population of design candidates, MOGAs can identify multiple Pareto solutions at the same time without specifying weights between objectives.

This paper considers the multipoint aerodynamic optimization of a wing shape for a SST at both supersonic and transonic cruise conditions. Aerodynamic drags will be minimized at both conditions under lift constraints. Bending moment at the root will also be minimized so as to prevent all the Pareto solutions having impractically large aspect ratios. In the aerodynamic optimization, design variables specify planform shapes, camber, thickness distributions and twist distributions. In the previous study, the same MO optimization was performed using a potential solver and an Euler solver under the inviscid flow assumption.[3] To consider more realistic flow fields such as a possible flow separation, the viscous effect is considered in the present optimization. Thus, a Navier-Stokes solver is used to evaluate the wing performance at both cruise conditions. Finally, the resulting Pareto solutions are analyzed and compared with NAL's design and the previous results.

2 OPTIMIZATION METHOD

Application of GAs to MO optimization has many advantages. Their advantages originate in the algorithms themselves, which imitate the mechanism of the natural evolution, where a biological population evolves over generations to adapt to an environment by selection, crossover and mutation. In design optimization problems, fitness, individual and genes correspond to an objective function, design candidate and design variables, respectively.

GAs search from multiple points in the design space simultaneously and stochastically, instead of moving from a single point deterministically like gradient-based methods. This feature prevents design candidates from settling in local optimum. Moreover, GAs do not require computing gradients of the objective function. These characteristics lead to following three advantages of GAs: 1, GAs have capability of finding global optimal solutions. 2, GAs can be processed in parallel. 3, high fidelity CFD codes can easily be adapted to GAs without any modification because GAs use only objective function values.

GAs have been extended to solve MO problems successfully.[2] GAs use a population to seek optimal solutions in parallel. This feature can be extended to seek Pareto solutions in parallel without specifying weights between the objective functions. The resultant Pareto solutions represent global tradeoffs. Therefore, MOGAs are quite unique and attractive methods to solve MO problems.

Figure 1 shows the flowchart of MOGAs in the present study. The following describes genetic operators employed here in brief. Traditionally, GAs use binary numbers to represent design parameter values. For real function optimizations like the present aerodynamic optimization, however, it is more straightforward to use real numbers. Thus, the floating-point representation is used here. Selection is based on the Pareto ranking method and fitness sharing.[2] Each individual is assigned to its rank according to the number of individuals that dominate it. A standard fitness sharing function is used to maintain the diversity of the population. To find the extreme Pareto solutions more effectively, the so-called best-N selection[4] is also coupled with. Blended crossover[5] (BLX-α) described below is adopted. This operator generates children on a segment defined by two parents and a user specified parameter α. In this optimization, a weighted average of new design variables is used as

$$
\begin{aligned}
\text{Child1} &= \gamma\cdot\text{Parent1} + (1-\gamma)\cdot\text{Parent2} \\
\text{Child2} &= (1-\gamma)\cdot\text{Parent1} + \gamma\cdot\text{Parent2} \\
\gamma &= (1 + 2\alpha)\cdot \mathit{ran1} - \alpha
\end{aligned} \tag{1}
$$

where Child1,2 and Parent1,2 denote encoded design variables of the children (members of the new population) and parents (a mated pair of the old generation), respectively. The random number shown here *ran1* is uniform in [0,1]. Parameter α is set to 0.5 except for the six planform design variables. Since the planform has a large impact on aerodynamic performance, its design parameters have to be given conservatively. Otherwise, the computation diverges and many children cannot be evaluated. Therefore, parameter α is set to 0.0 for those six design variables. Mutation takes place at a probability of 20%. If the mutation occurs, then Eqs. (1) will be replaced by

$$
\begin{aligned}
\text{Child1} &= \gamma\cdot\text{Parent1} + (1-\gamma)\cdot\text{Parent2} + m\cdot(\mathit{ran2}-0.5) \\
\text{Child2} &= (1-\gamma)\cdot\text{Parent1} + \gamma\cdot\text{Parent2} + m\cdot(\mathit{ran2}-0.5)
\end{aligned} \tag{2}
$$

where *ran2* are also uniform number in [0,1] and *m* is set to 10% of the given range of each design variable.

Objective functions for each individual are to be evaluated using a CFD solver. In order to evaluate the viscous effect, the three-dimensional Navier-Stokes equations should be solved. In this study, the three-dimensional, compressible, thin-layer Navier-Stokes solver is used to evaluate aerodynamic performances in both transonic and supersonic cruise conditions. This Navier-Stokes code employs total-variation-diminishing type upwind differencing and the lower-upper factored symmetric Gauss-Seidel scheme.[6] The multigrid method[7] is also used to accelerate the convergence. The turbulence model in this code adopts an algebraic mixing length model by Baldwin and Lomax.[8]

3 FORMULATION OF THE PRESENT OPTIMIZATION PROBLEM

The present optimization problem can be stated as follows.

[Objective functions]

1. Drag coefficient for transonic cruise, $C_{D,t}$
2. Drag coefficient for supersonic cruise, $C_{D,s}$
3. Bending moment at the wing root for supersonic cruise condition, M_{root}

[Constraints]

1. Lift coefficients, $C_{L,t}$ = 0.15 and $C_{L,s}$ = 0.10 at cruise conditions
2. Wing area, S = 60
3. Maximum airfoil thickness, $t/c \geq 0.03$

[Flow conditions]

1. Transonic cruising Mach number: 0.9
2. Supersonic cruising Mach number: 2.0
3. Reynolds number based on the root chord length at both conditions: 1.0×10^7

In the present optimization, all the three objective functions are to be minimized. Both the supersonic and transonic drag coefficients are evaluated by using a Navier-Stokes flow solver. The bending moment is computed by directly integrating the pressure load at the supersonic cruise condition. To maintain lift coefficients constant, the angle of attack is predicted by using $C_{L\alpha}$ obtained from the finite difference. Thus, three Navier-Stokes computations are performed per evaluation. During the aerodynamic optimization, wing area is frozen at a constant value. The wing thickness is also constrained for structural strength.

Design variables are categorized to planform, airfoil shapes and the wing twist. The wing planform is determined by six design variables as shown in Fig. 2 and their ranges are written in Table 1. A chord length at the wing tip is determined accordingly because of the fixed wing area. Airfoil shapes are composed of its thickness distribution and camber line. The thickness distribution is represented by a Bezier curve defined by nine polygons[9] as shown in Fig. 3. Table 1 also shows their design ranges. The thickness distributions are defined at the wing root, kink, and tip and then linearly interpolated in the spanwise direction. The total number of polygons is 27 for the entire thickness distribution. The camber surfaces composed of the airfoil camber lines are defined at the inboard and outboard of the wing separately. Each surface is represented by the Bezier surface defined by four polygons in the chordwise direction and three in the spanwise direction. For instance, Figure 4 shows the camber line with its control points at the root. It is concave only at the root and it becomes convex at the other spanwise locations similar to the warp design based on the linearized theory. The number of polygons that defines two camber surfaces is 20 polygons in total. Finally, the wing twist is represented by a B-spline curve with six polygons as shown in Fig. 5. As a result, 66 design variables are used to define a wing shape.

The present optimization was performed on FUJITSU VPP700E supercomputer system at The Institute of Physical and Chemical Research. The system has 160 PE's with 384 GFLOPS and 320 GB. The master PE manages MOGA, while the slave PE's compute the

Navier-Stokes code. The population size was set to 64 so that the process was parallelized with 8-64 PE's depending on the availability. It should be noted that the parallelization was almost 100% because of the Navier-Stokes computations dominated the CPU time.

4 OPTIMIZATION OF A SUPERSONIC TRANSPORT WING

4.1 Overview of Pareto solutions

The evolution was computed for 30 generations. After the present optimization by MOGA, all the solutions evaluated were sorted again to find Pareto solutions as much as possible. As a result, the final Pareto solutions were obtained in the three-dimensional objective function space as shown in Fig. 6. The tradeoff surface with the objective functions is exhibited in the figure. It also shows four typical planform shapes; $C_{D,t}$ minimum, $C_{D,s}$ minimum, bending moment minimum and a certain Pareto solution. The extreme Pareto solutions, three planform shapes that minimize the respective objective functions appear physically reasonable.

To present tradeoffs between the objectives more clearly, Pareto solutions are projected into the two-dimensional plane as shown in Figs. 7-9. Figures 7 and 8 present the tradeoffs between transonic and supersonic drag coefficients. The solutions are labeled by the aspect ratio, and the taper ratio using different symbols in Figs. 7 and 8, respectively. In Fig. 7, wings with larger aspect ratios achieve lower drag coefficients as expected in the aerodynamic theory. Figure 8 shows that the wings that have the taper ratios smaller than 0.4 have good aerodynamic performances, but further decrease of the taper ratio does not correspond to the reduction of cruising drag directly. On the other hand, the wings with the taper ratios larger than 0.4 have the lower bending moments and poor aerodynamic performances as shown in Fig. 9.

4.2 Comparison with NAL's second design

To examine the quality of the present Pareto solutions, two Pareto solutions are compared with NAL's second design. NAL SST Design Team already finished the fourth aerodynamic design for the experimental supersonic airplane to be launched in 2002. To summarize their design concepts briefly, the first design determined the planform shapes among 99 candidates, and then the second design was performed by the warp optimization based on the linearized theory. The third design aimed a natural-laminar-flow (NLF) wing by an inverse method using a Navier-Stokes code. Finally, the fourth design was performed for a wing-fuselage configuration. Because a fully developed turbulence is assumed in the present Navier-Stokes computations, it is improper to compare the present Pareto solutions to NAL's NLF wing design. Therefore, the NAL second design is chosen for a comparison.

Table 2 summarizes comparisons of two Pareto solutions with NAL's second design. The aerodynamic calculation of NAL's second design is performed here by using the same Navier-Stokes solver. Pareto solutions A and B presented here are superior to NAL's second design in all three objectives. Figure 10 shows the wing planforms of the three, indicating a large difference of planform shapes between the present solutions and NAL's design. The present planforms are similar to the “arrow wing” planform and the NAL's planform is similar to the conventional “delta wing” planform.

The thickness distributions of the three wings are shown in Fig. 11. The trend of thickness distributions of Pareto solutions A and B are quite similar, having a blunt leading edge and a thin trailing edge. The thickness distribution of NAL's design is simply taken from an existing NLF airfoil. In contrast, the present optimization is performed under a fully turbulent flow with the thickness constrained. Therefore, the maximum thickness appears near the leading edge. Then, the thickness is reduced toward the trailing edge to prevent the rapid growth of the boundary layer.

4.3 Difference between the viscous and inviscid calculations

The present viscous designs are compared with the inviscid designs computed previously.[3] By comparing the two optimization results, the difference of the wing shapes due to the viscous effect becomes clear. The Pareto solutions, which are found to outperform NAL's design in all three objectives at both cases, are selected for the comparison.

A comparison of the planform shapes is shown in Fig. 12. Both planform shapes are similar to the “arrow wing” planform, but the shapes are slightly different. The present wing has a less sweep angle and a less taper ratio than the optimized wing under the inviscid flows. A highly swept wing tends to have a flow separation near the wing tip. The present viscous design appears better than the inviscid design to prevent the tip separation.

Figure 13 shows a comparison of the thickness distributions at the root. It shows the quite different distributions. In the viscous case, the wing is thicker near the leading edge and thinner near the trailing edge. However, in the inviscid case, the wing is very thick. The C_p distributions shown in Fig. 14 explain their difference clearly. In the inviscid case, the C_p distribution has a discontinuity at the trailing edge, and therefore it generates the lift even at the trailing edge. However, such a thick airfoil probably causes a flow separation. On the other hand, there is no discontinuity at the trailing edge for the viscous flow case. It is important to consider the viscous effect for designing thickness distributions.

5 CONCLUSION

The multipoint design optimization of a wing for a SST has been performed by using MOGA. Three objective functions are used to minimize the supersonic drag, the transonic drag and the bending moment at the wing root. The complete wing shape is represented by in total of 66 design variables. The Navier-Stokes solver is used to evaluate those aerodynamic drags.

Successful optimization results are obtained. The planforms of the extreme Pareto solutions appear physically reasonable. Global tradeoffs between the objectives are presented. Two Pareto solutions have better performance in all three objective functions compared with NAL's second design. The comparison of the present Pareto solution with the optimal wing designed previously under the inviscid flow is also carried out to examine the viscous effect. The viscous effect is found to have a large influence on the thickness distribution. The present result is found better to prevent the possible boundary layer separation. The analysis of the Pareto solutions suggests that a desirable planform shape is a new type of the arrow wing with a relatively large taper ratio and a relatively small aspect ratio similar to the previous inviscid results.

ACKNOWLEDGMENTS

This research was partly funded by Japanese Government's Grants-in-Aid for Scientific Research, No. 10305071. The second author's research has been partly supported by Bombardier Aerospace, Toronto, Canada. The computational time was provided by The Institute of Physical and Chemical Research. The authors would like to thank National Aerospace Laboratory's SST Design Team for providing many useful data.

REFERENCES

[1] T. Iwamiya, "NAL SST Project and Aerodynamic Design of Experimental Aircraft", *4th ECCOMAS Computing Fluid Dynamics Conference*, **2**, John Wiley & Sons, 580-585

(1998).

[2] C. M. Fonseca and P. J. Fleming, “Genetic algorithms for multiobjective optimization: formulation, discussion and generalization”, *5th International Conference on Genetic Algorithms*, Morgan Kaufmann Publishers, 416-423 (1993).

[3] S. Obayashi, D. Sasaki, Y. Takeguchi and N. Hirose, “Multiobjective Evolutionary Computation for Supersonic Wing Shape Optimization”, *IEEE Transactions on Evolutionary Computation*, in print.

[4] S. Obayashi, S. Takahashi and Y. Takeguchi, “Niching and Elitist Models for MOGAs”, *Parallel Problem Solving form Nature – PPSN V*, Lecture Notes in Computer Science, Springer, 260-269 (1998).

[5] L. J. Eshelman and J. D. Schaffer, “Real-coded genetic algorithms and interval schemata”, *Foundations of Genetic Algorithms 2*, Morgan Kaufmann Publishers, 187-202 (1993).

[6] S. Obayashi and G. P. Grurswamy, “Convergence Acceleration of a Navier-Stokes Solver for Efficient Static Aeroelastic Computations”, *AIAA Journal*, **33**, 1134-1141 (1995).

[7] A. Jameson and D. A. Caughey, “Effect of Artificial Diffusion Scheme on Multigrid Convergence”, AIAA Paper 77-635 (1977).

[8] B. S. Baldwin and H. Lomax, “Thin layer Approximation and Algebraic Model for Separated Turbulent Flows”, AIAA Paper 78-257 (1978).

[9] R. Grenon, “Numerical Optimization in Aerodynamic Design with Application to a Supersonic Transport Aircraft”, *Int. CFD Workshop for Super-Sonic Transport Design*, National Aerospace Laboratory, 83-104 (1998).

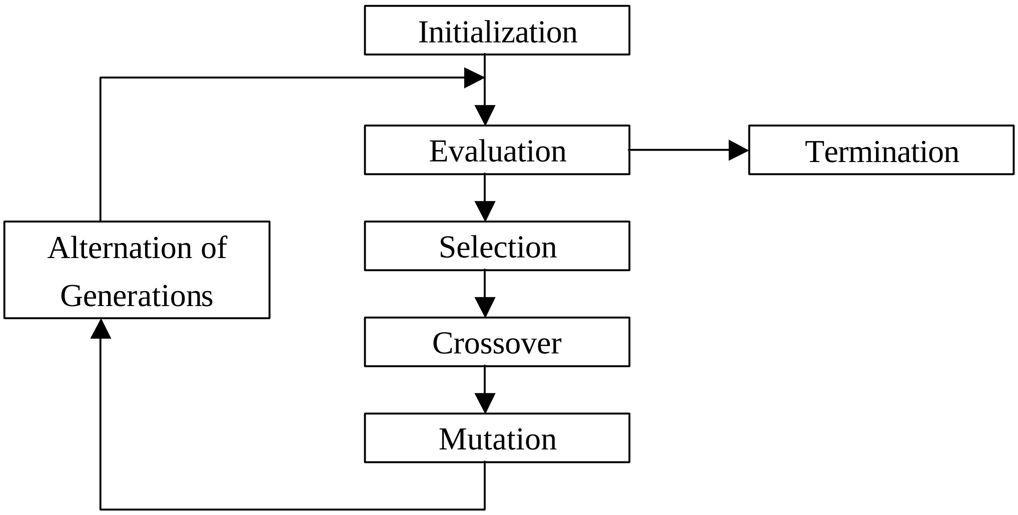

Figure 1: Flowchart of GAs

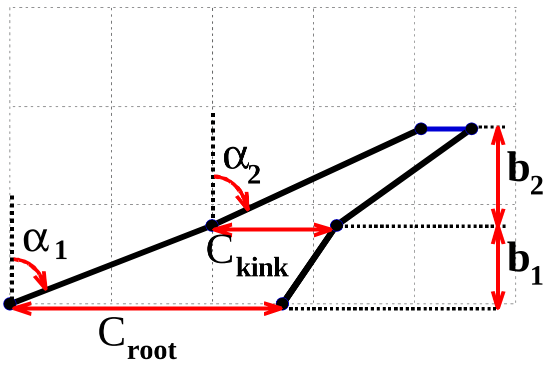

Figure 2: Wing planform definition

Planform shape		
Chord length	C_{root}	10-20
	C_{kink}	3-15
Span length	b_1	2-7
	b_2	2-7
Sweep angle (deg)	α_1	35-70
	α_2	35-70
Thickness distribution		
Max thickness (%)	Zp_4	3-4
Max thickness location (%)	Xp_4	15-70

Table 1: Ranges of planform and thickness distribution design variables

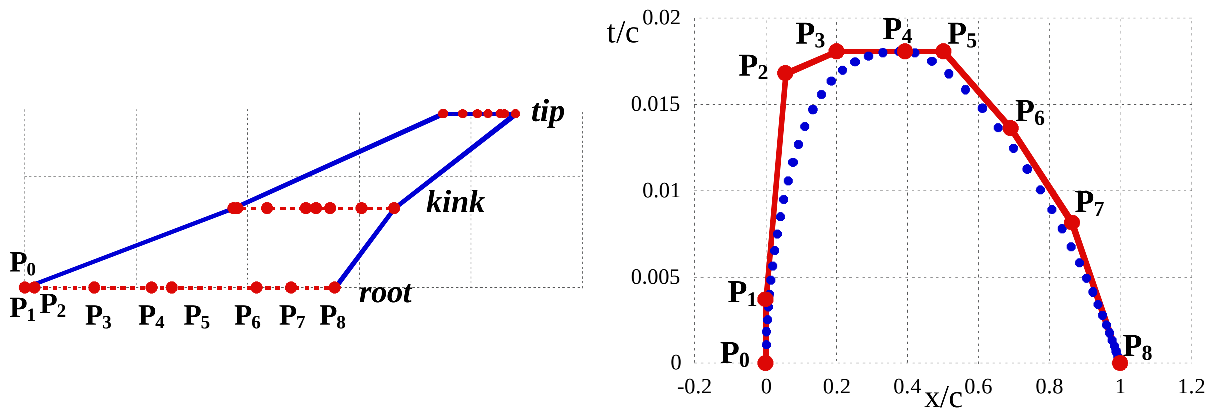

Figure 3: Wing thickness definition

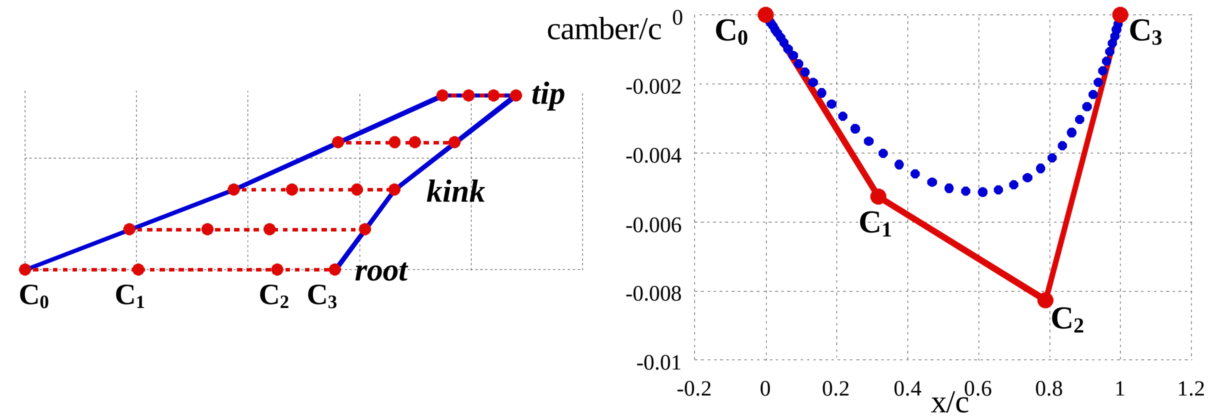

Figure 4: Wing camber definition

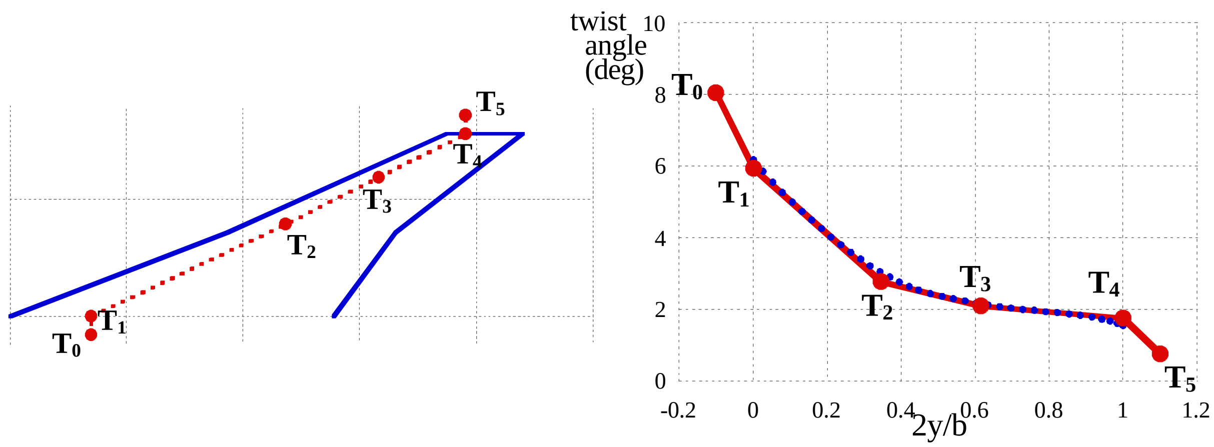

Figure 5: Wing twist definition

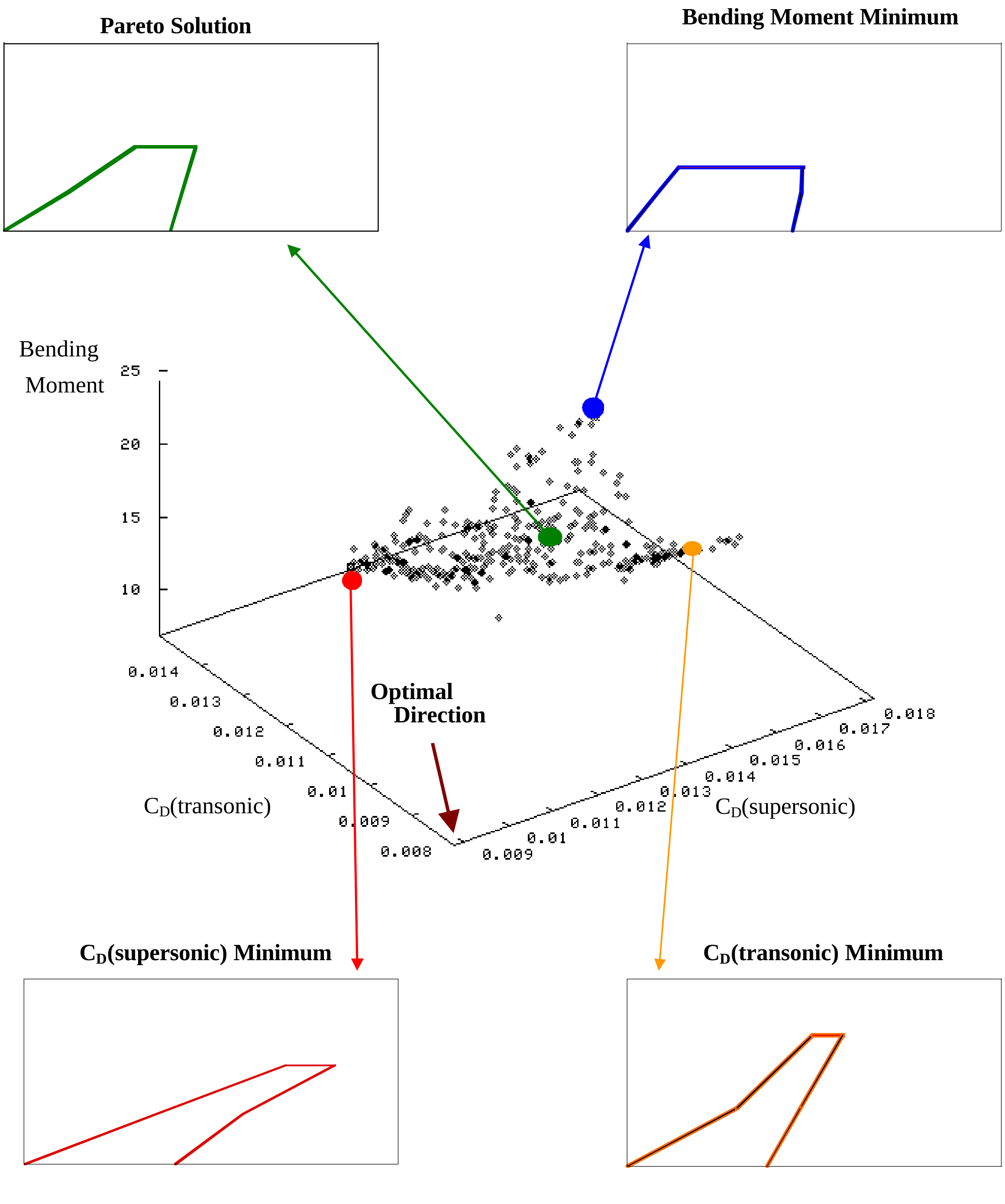

Figure 6: Pareto front in the objective function space and typical planform shapes

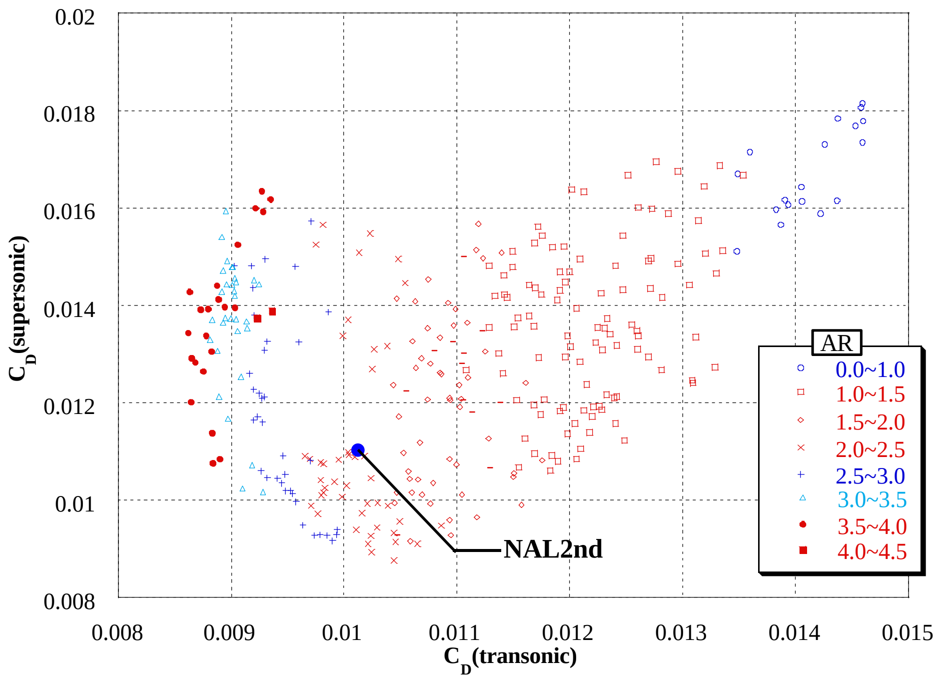

Figure 7: Projection of Pareto front to supersonic and transonic drag tradeoffs labeled according to aspect ratios. NAL's design is plotted here for a comparison although it is not Pareto optimal.

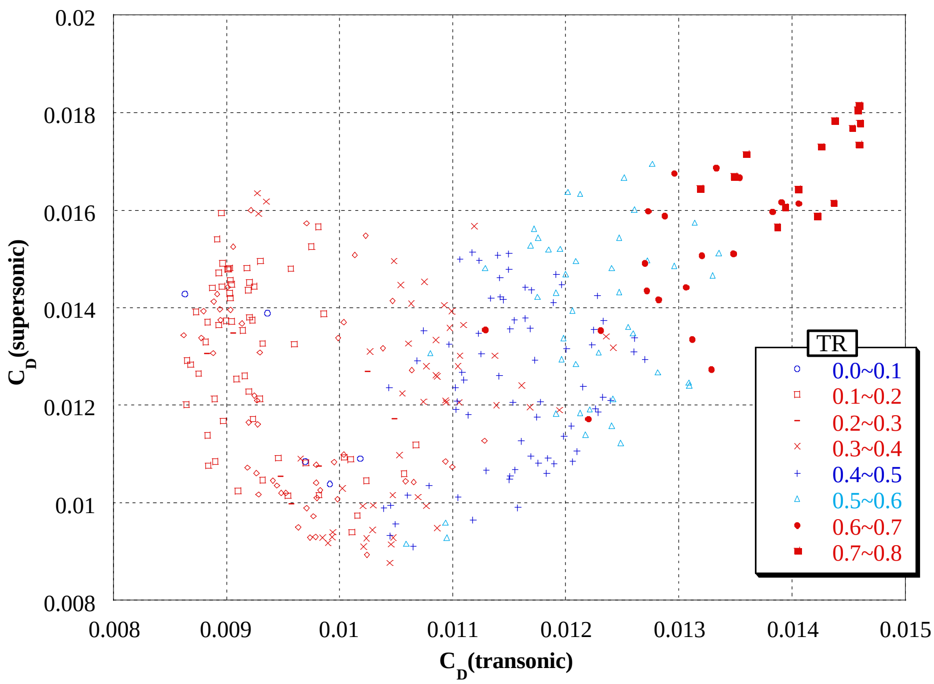

Figure 8: Projection of Pareto front to supersonic and transonic drag tradeoffs labeled according to taper ratios

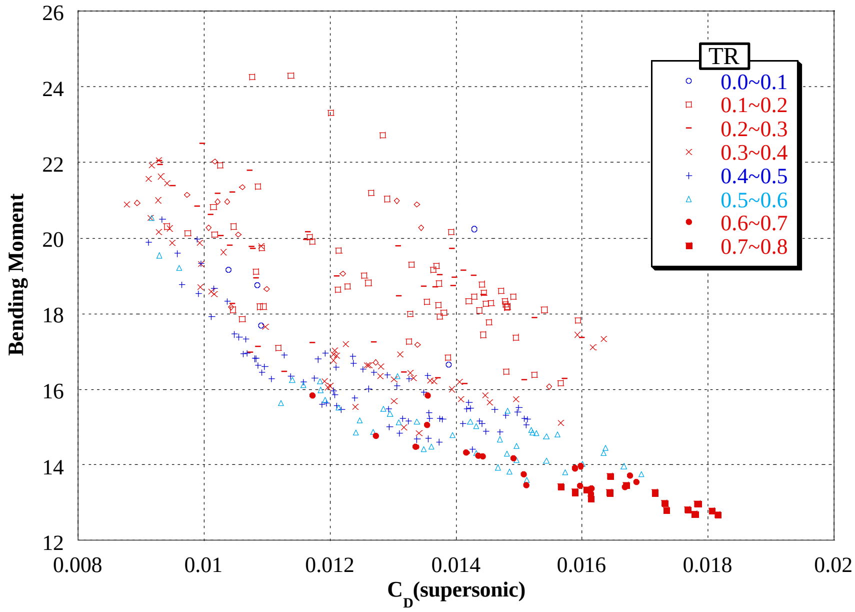

Figure 9: Projection of Pareto front to bending moment and supersonic drag tradeoffs labeled according to taper ratios

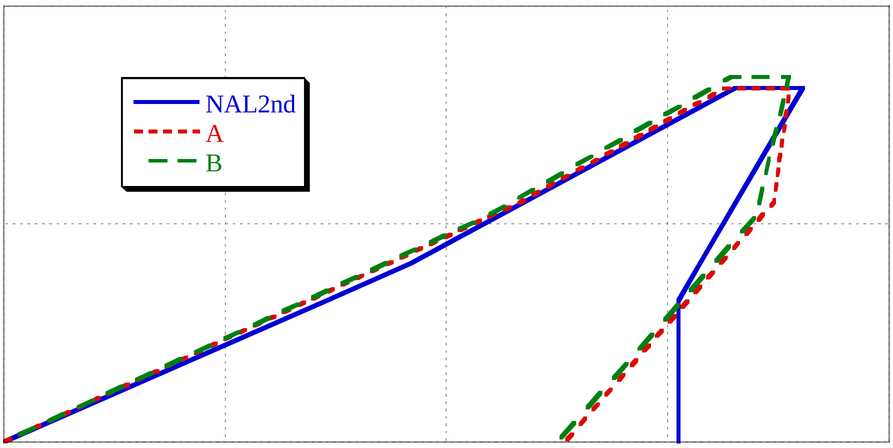

Figure 10: Comparison of planform shapes between selected Pareto solutions and NAL's design

	Aspect Ratio	Taper Ratio	C_D(transonic) ($\times10^{-4}$)	C_D(supersonic) ($\times10^{-4}$)	Bending Moment
A	2.19	0.12	100.40	109.38	18.18
B	2.34	0.11	100.96	108.89	18.18
NAL2nd	2.20	0.20	100.99	110.92	18.52

Table 2: Performance comparison among selected Pareto solutions and NAL's design

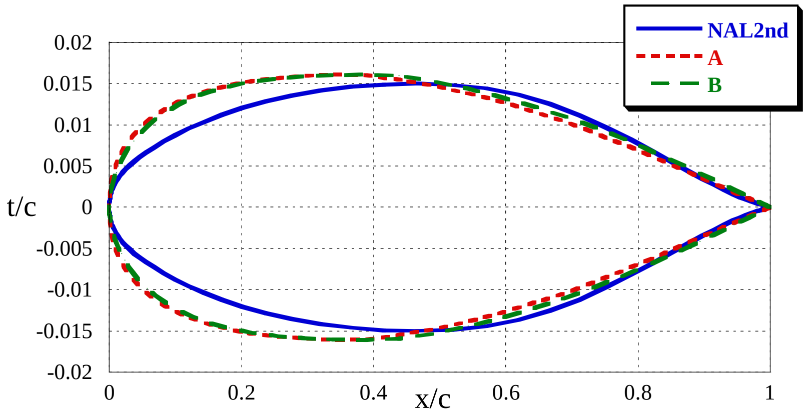

c) 66% spanwise location

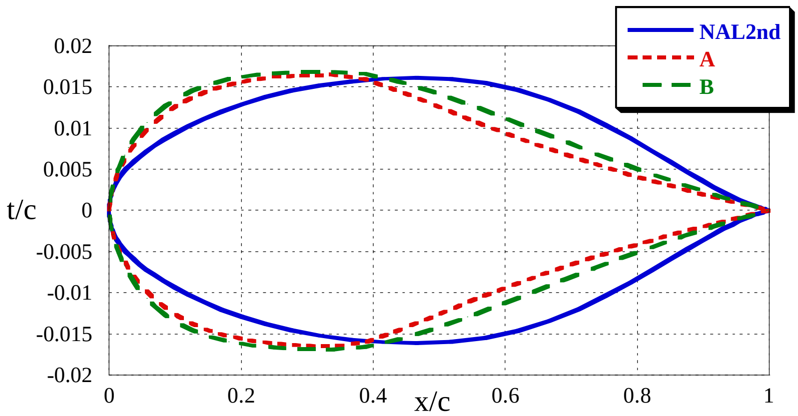

b) 33% spanwise location

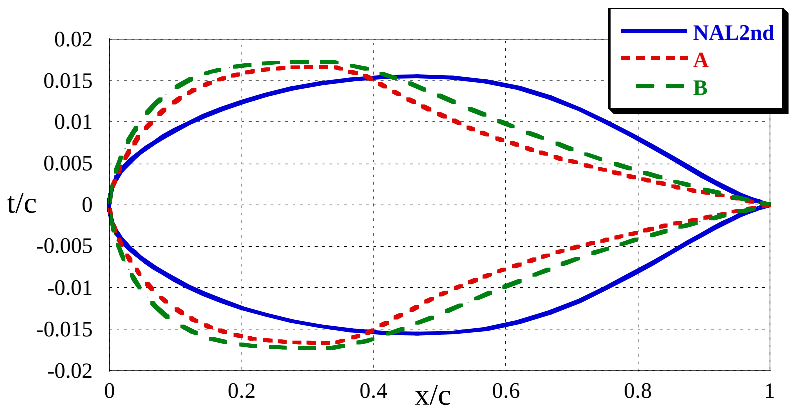

a) 0% spanwise location

Figure 11: Comparison of thickness distributions between selected Pareto solutions and NAL's design

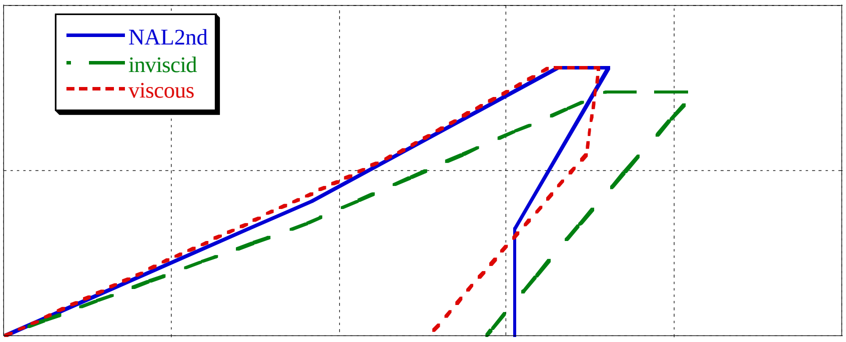

Figure 12: Comparison of planform shapes of the viscous and inviscid designs with NAL's design

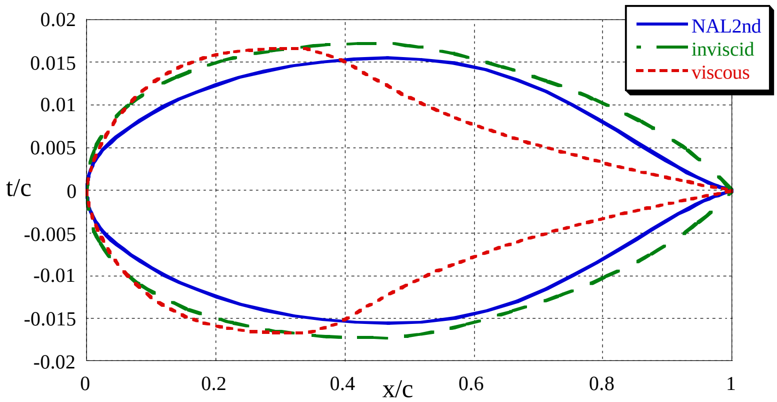

Figure 13: Comparison of thickness distributions of the viscous and inviscid designs with NAL's design

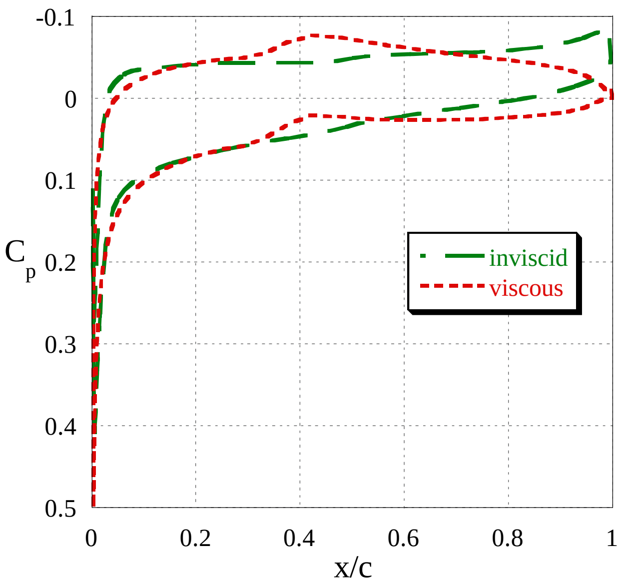

Figure 14: Comparison of C_p distributions of the viscous and inviscid designs with NAL's design